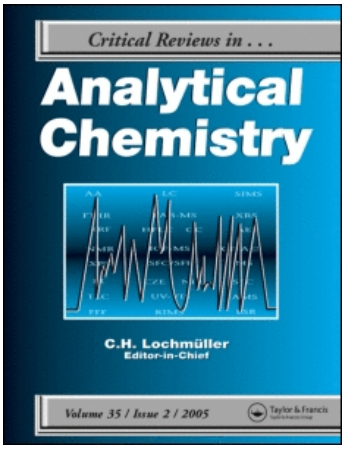

Critical Reviews in Analytical Chemistry
Publication details, including instructions for authors and subscription information:
http://www.informaworld.com/smpp/title~content=t713400837

Variable Exit Angle X-Ray Fluorescence Spectroscopy

Tom Scimeca[a]
[a] Department of Chemistry at the University of Hawaii, Honolulu

To cite this Article Scimeca, Tom(1989) 'Variable Exit Angle X-Ray Fluorescence Spectroscopy', Critical Reviews in Analytical Chemistry, 21: 3, 225 — 235
To link to this Article: DOI: 10.1080/10408348908050845
URL: http://dx.doi.org/10.1080/10408348908050845

Variable Exit Angle X-Ray Fluorescence Spectroscopy

Tom Scimeca

I. INTRODUCTION

The study of thin films and surfaces has received increasing attention over the last 10 years. Furthermore, there has been an increasing number of techniques devoted to these studies.[1] The majority of the techniques achieve their surface sensitivity as a result of the strong coupling between the charged particle and the material that the particle traverses before it is detected. For example, with electron detection techniques (e.g., photoemission [XPS,UPS] and Auger electron spectroscopy [AES]), this strong coupling leads to an electron mean free path that ranges from 5 to 30 Å for most materials in the electron energy range of 10 to 1000 eV.[2]

While the charged particle surface-thin film techniques have been remarkably successful in fundamental studies for systems that are well suited to their limitations (e.g., chemisorption), the bridge between ideal and real systems is, at best, rather tenuous[3] (e.g., chemisorption-catalysis). Furthermore, these charged particle techniques rely almost exclusively on destructive techniques to sample depth profile.

Recently, however, a number of photon in-photon out techniques have also been used to nondestructively study thin films and surfaces.[4-7] These techniques have achieved their surface sensitivity and depth profiling capability by operating in a grazing incidence mode. In particular, these X-ray grazing techniques are surface sensitive when the incident angle is less than the critical angle while a drastic change in the X-ray penetration depth occurs when the incident angle is varied near the X-ray critical angle. Therefore, by changing the incident angle near the critical angle, a great deal of depth profiling can be achieved within a very small angular range. However, this article focuses on achieving depth profiling capability in the grazing exit angle mode hereafter denoted variable exit angle X-ray fluorescence spectroscopy (VEAXFS). One reason for operating in this mode is that a minimum of effort is required to modify the wavelength dispersive instrument described later in the text. Furthermore, both elemental and chemical bonding information[8,9] can be obtained while depth profiling.

The basic idea behind the VEAXFS technique has been discussed elsewhere[10,11] and reviewed from a slightly different perspective elsewhere.[11] The surface enhancement is achieved by varying the sample geometry with respect to either the incident or exit X-rays (or both). By varying the sample geometry, one varies the normal component to the X-ray escape depth thereby changing the surface enhancement, as shown in Figure 1.

It should be mentioned that grazing incidence X-ray fluorescence[7,12] and variable energy X-ray emission[13-15] have been utilized in the past to nondestructively depth profile. The grazing incidence XRF technique has been shown to be a powerful tool for nondestructive depth profiling with quantitative accuracy. This technique uses a Si(Li) detector. Furthermore, by tuning the incident photon energy near the analyte absorption edge, chemical speciation can be realized.[12] This technique is known as selectively induced X-ray emission (SIXES). While SIXES has been applied to thin film analysis, it has not been used to sample depth profile — owing largely to the sensitivity of the energy dependent X-ray penetration depth. Nevertheless, the potential of this technique has yet to be realized. The X-ray emission studies of Holliday[13] and Szasz and Kojnok[14] achieve depth profiling capability by varying the electron energy used to excite the characteristic X-rays.

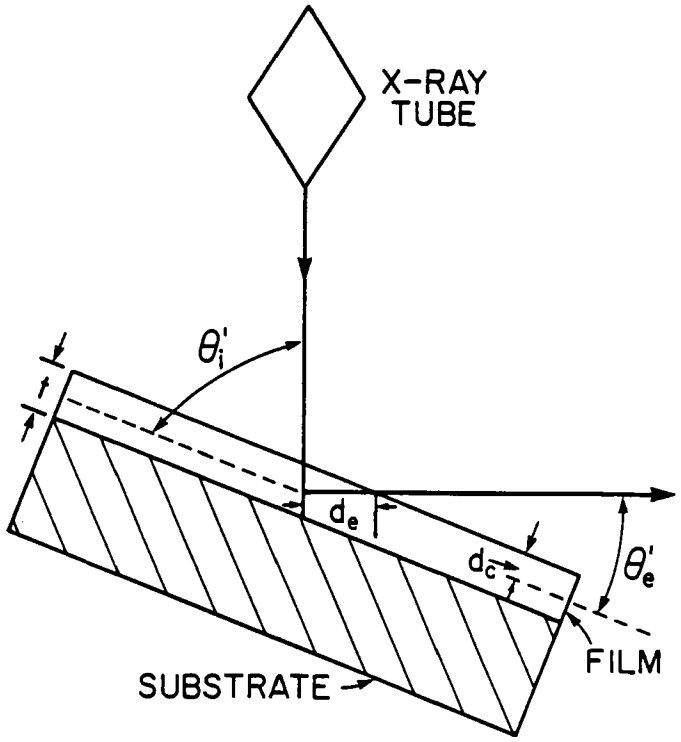

FIGURE 1. The incident and exit angle are shown in this figure for a hypothetical multilayer sample consisting of five discrete thin films.

Finally, the XFS work presented here focuses on the soft X-ray region ($\lambda > 10$ Å) in contrast to the hard X-ray region ($\lambda < 2$ Å). While, in general, relatively little work is done in this energy region, there are a number of advantages in this region when the VEAXFS technique is applied to quantitative analysis of thin films. For example, in addition to being more sensitive to thin films (for thin film thicknesses of up to around 1000 Å), enhancement and secondary scattering can usually

Tom Scimeca received a B.S. Ch.E. from the University of Illinois, Urbana-Champaign. Currently, he is Graduate Assistant in the Department of Chemistry at the University of Hawaii, Honolulu.

be safely ignored. This is discussed later in this paper. It should be mentioned that XRF work in the hard X-ray region for thin films and multilayers including enhancement have met with success,[16-18] at the expense of convenience and computational expense. However, it should be stated that in the hard X-ray region, one has the advantage of not requiring a vacuum and the fluorescence yield is higher in this energy range.

II. SURFACE ENHANCEMENT BY THE VEAXFS TECHNIQUE

The surface sensitivity of the VEAXFS technique can best be seen by calculating the distribution of secondary X-ray fluorescence emanating from a sample as a function of exit angle. The intensity distribution is derived from ordinary X-ray fluorescence equations[19] where the differential intensity of analyte A is given by

$$dI_A = I_o[\exp(-\alpha\rho_i t)_A]\rho_A \csc\theta_i K_A dt \quad (1)$$

where

$$\alpha_A = (\mu_{i,A})\csc\theta_i + (\mu_{e,A})\csc\theta_e$$

$$K_A = C_A(\mu_{i,A})((r_A - 1)/r_A)(\omega_A)g_L\left(\frac{d\Omega}{4\pi}\right)$$

In the previous equation, dI_A is the differential intensity for element A in the jth layer of thickness dt, I_o is the incident flux, ρ_A is the density of analyte A and $\mu i,A$ and $\mu e,A$ are the mass absorption coefficients of the incident and exit X-rays in analyte A. The K_A term contains the concentration term (1.0 in our case), the jump ratio r_A, the fluorescence yield w_A, the electron degeneracy g_L, and the fraction of photons collected by the detector ($d\Omega / 4\pi$). To calculate the distribution, one starts by considering the intensity ratio for a differential thickness within the sample (dt) with respect to the same differential thickness at the sample surface (dt_s). The intensity ratio is

$$\frac{I_t}{I_s} = \exp(-\alpha\rho' t_i)\left[\frac{1 - \exp(-\alpha\rho dt_i)}{1 - \exp(-\alpha\rho dt_s)}\right] \quad (2)$$

where ti is the depth within the sample. Equation 2 can be further simplified to

$$\frac{I_t}{I_s} = \exp(-\alpha\rho t_i) \quad (3)$$

since $dt = dt_s$.

In Figure 2, the Ni Lα intensity distribution is plotted for various exit angles. For this plot, as well as the other theoretical plots presented in this article, the soft X-ray absorption coefficient values from Henke's tabulation[20] are used.

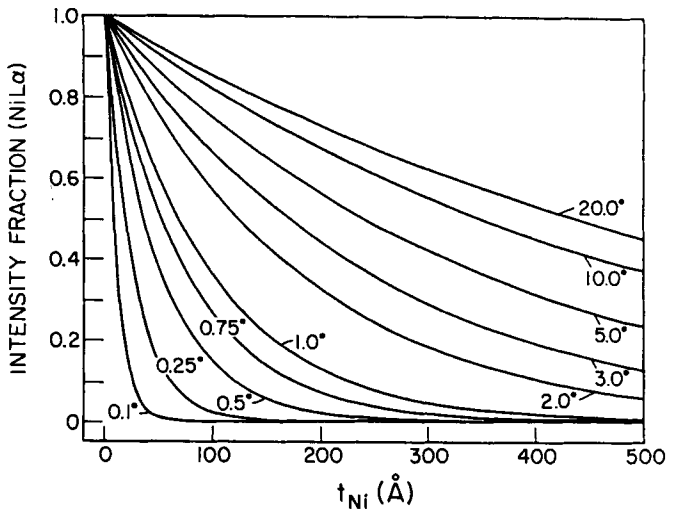

FIGURE 2. The Ni Lα intensity distribution is plotted for various exit angles for Ni thicknesses extending to 500 Å.

The X-ray intensity distribution for thin film multilayers is also straightforward. For example, the X-ray intensity distribution for a multilayer system consisting of two similar discrete thin films of thickness t_1 and t_2 separated by a different neutral filter thin film tnf is given by

$$\frac{I_{t,i}}{I_{t,s}} = \exp(-\alpha\rho t_i)_i \exp(-\alpha\rho t)_{nf} \quad (4)$$

where $ti < t_1 + t_2$ and the neutral attenuation factor is included only if $ti > t_2$. The Ni Lα intensity distribution for a Ni/Fe/Ni thin film system, where each thin film thickness is 150 Å, is plotted for various exit angles in Figure 3. One can see from

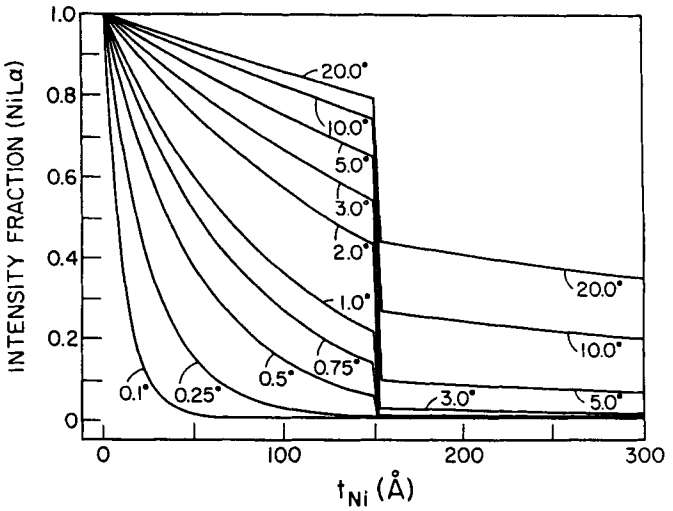

FIGURE 3. The Ni Lα intensity distribution for a 150 Å Ni/150 Å Fe/150 Å Ni multilayer thin film sample for various exit angles is plotted.

this plot how the X-ray intensity from the interfacial region varies when the exit angle is changed illustrating the capability of this technique for studying buried interfaces. A more concise way of expressing the depth from which the X-rays emanate can also be calculated. This depth is known as the X-ray critical depth and is worked out in detail by Scimeca and Andermann.[21] Finally, it should be mentioned that there have been a number of assumptions made in this theoretical analysis. These assumptions are

1. Monochromatic incident beam.
2. Each layer (thin film) is homogeneous in all directions.
3. Each layer is discrete.
4. Self enhancement is ignored (w is small-a valid assumption in the soft X-ray region).[22]
5. The sample is perfectly smooth.[21,23]
6. Refractive index effects are ignored. In fact, the angles used here are internal angles within the sample such that even with refractive index effects, the equations are still valid.[21]
7. No differential contamination between the thin film and its reference (except where mentioned).
8. Elastic (and inelastic) photon scattering is negligible.[20]

The validity of these assumptions depends on the X-ray source (Assumption 1), the X-ray energy region one works in (Assumptions 4,8), sample cleanliness (Assumption 7), as well as the sample perfection (Assumptions 2,3, and 5). These assumptions are also used in the theoretical treatment of the following section and are discussed in more detail in the experimental results section of this article. It should also be mentioned that the calculations have all relied on pure materials. However, the equations are valid for uniform thin films where the concentration of the analyte is not 100%. In this case, one needs to modify several terms in Equation 1.

III. THEORETICAL TREATMENT

A. The External Standard Intensity Ratio (ESIR)

The details of the ESIR technique have been worked out by Scimeca and Andermann.[24] The ESIR treatment begins by integrating Equation 1 over the thickness of the thin film yielding

$$I_A = [1 - \exp(-\alpha\rho t)_A]\left[I_o K_A \rho_A \frac{\csc\theta_i}{\alpha_A \rho_A}\right] \quad (5)$$

The ESIR is then

$$\frac{I_A}{I_{A,tr}} = \left[\frac{1 - \exp(-\alpha\rho t)_A}{1 - \exp(-\alpha\rho_i t_r)_A}\right] \quad (6)$$

where tr is the reference thickness. Equation 6 can be further simplified if tr is infinitely large [i.e., $\exp(-\alpha\rho tr) << 1$]. In this case, one obtains

$$\frac{I_A}{I_{A,\infty}} = 1 - \exp(-\alpha\rho t)_A \quad (7)$$

The ESIR technique can also be readily applied to multilayers. If tr = ∞, the characteristic intensity contribution from the jth layer, as indicated in Figure 1, relative to the jth layer bulk reference is

$$\frac{I_A}{I_{A,\infty}} = (F_{i,j})(F_{e,j})[1 - \exp(-\alpha\rho t)_A] \quad (8)$$

where Fi,j and Fe,j are the incident and exit attenuation factors for layer J given by

$$F_{i,j} = \prod_{K=1}^{J-1} \exp(-\mu_{i,k}\rho_k \csc\Theta_i t_k)$$

$$F_{e,j} = \prod_{K=1}^{J-1} \exp(-\mu_{e,k}\rho_k \csc\Theta_e t_k)$$

The ESIR for Ni Lα radiation excited by Cu L (θi + θe = 90 is plotted in Figure 4 as a function of θe for a varying Ni thickness (top layer) ranging from 50 to 1000 Å. One can see from this plot that surface enhancement, as manifested in an increasing ESIR for a given Ni thickness, is realized at low exit angles. This type of curve also illustrates that, in the soft X-ray region, one can in principle determine the Ni thickness with a reasonable amount of precision. As one moves to harder

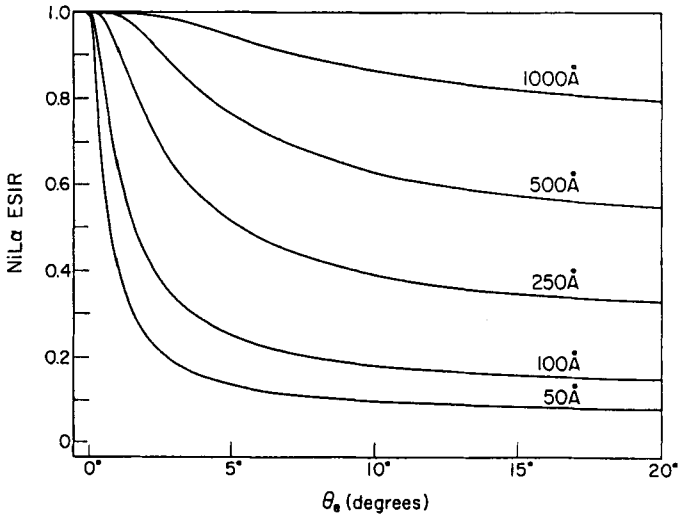

FIGURE 4. The Ni Lα external standard intensity ratio (ESIR) is plotted as a function of exit angle for various Ni thicknesses.

(lower) X-rays, the depth from which the X-rays emanate increases and the depth resolution decreases as a result of the decreased stopping power of the harder X-rays. This can be qualitatively seen in Figure 5 which is a plot of the Ni Kα intensity as a function of exit angle for Ni thin films ranging in thickness from 500 to 20,000 Å.

The ESIR for a thin film beneath an overlaying neutral thin film is given by Equation 8. One would expect the intensity contribution of the underlying thin film to decrease, relative to its reference, as the exit angle decreases (for a given overlying thin film thickness) and as the overlying thin film thickness increases. This is indeed the case, as one can see in Figure 6, for the two layer thin film system consisting of a varying Ni thickness over 150 Å of Fe.

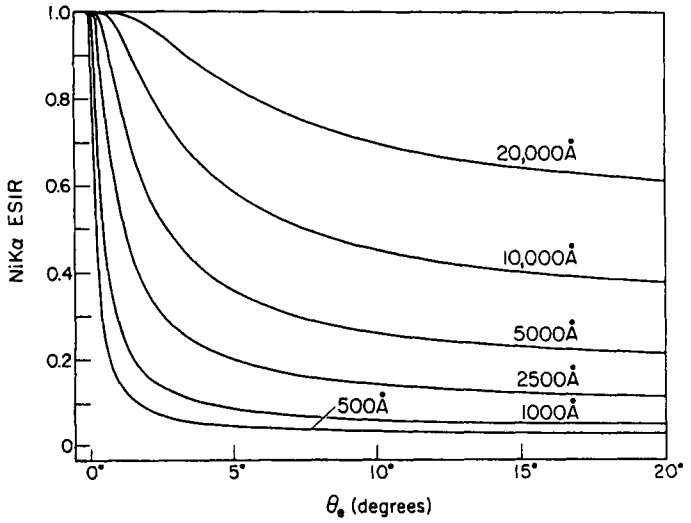

FIGURE 5. The Ni Kα ESIR is plotted as a function of exit angle for various Ni thicknesses.

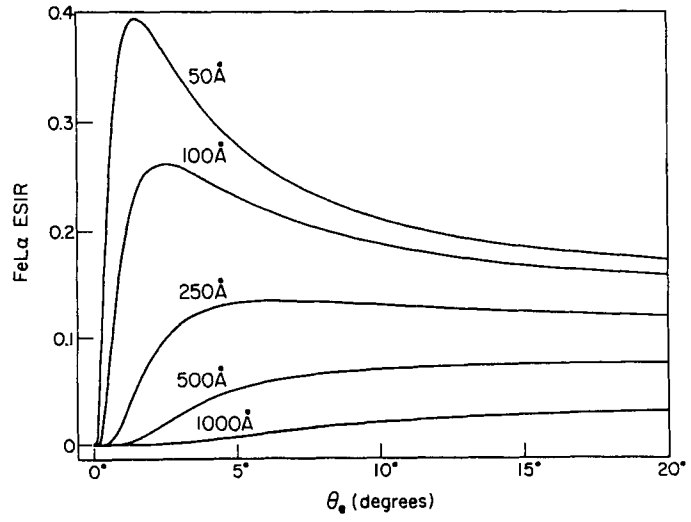

FIGURE 6. The Fe Lα ESIR is plotted as a function of exit angle for various Ni overlayer thicknesses and for a Fe thickness of 150 Å.

Another type of neutral filter which overlays the sample is surface contamination.[24] Calculating the ESIR intensity attenuation as a result of a contaminant overlayer begins with Equation 7 and is given by

$$\frac{I_A}{I_{A,\infty}} = \exp(*(\mu_{i,c}\csc\theta_i + \mu_{e,c}\csc\theta_e)\rho_c dt_c)[1 - \exp(-\alpha\rho t)_A] \quad (9)$$

where ρ_c and dtc are the density and differential thickness of the contaminant layer and μe,c and μi,c are the exit and incident mass absorption coefficients in the contaminant layer. If the * sign is positive, this indicates preferential contamination on the thin film reference, whereas a negative sign indicates the reverse situation.

The sensitivity of the preferential contamination on a Ni thin film referenced to bulk Ni(tr = ∞) is illustrated in Figure 7. The contaminant was taken to be a CH_2 polymer (ρ_c = 1.0). One can see that the disparity between the ISIR with and without preferential contamination increases as dtc increases and as the exit angle decreases, as expected.

B. The Internal Standard Intensity Ratio (ISIR)

The ISIR technique has several advantages over the ESIR technique. One of these advantages concerns the problem of preferential contamination mentioned previously. The ISIR method involves taking an intensity ratio between two types of thin films (or one thin film and a substrate) that are both within the same sample. The details of this treatment are worked out in Reference 24. One starts with Equation 5 with the exception that the thin film intensity is ratioed to a thin film of a different type within the same sample. Due to this, the intensity ratio must be modified since the fluorescence yield, cross section, detection efficiency, etc. (terms in the funda-

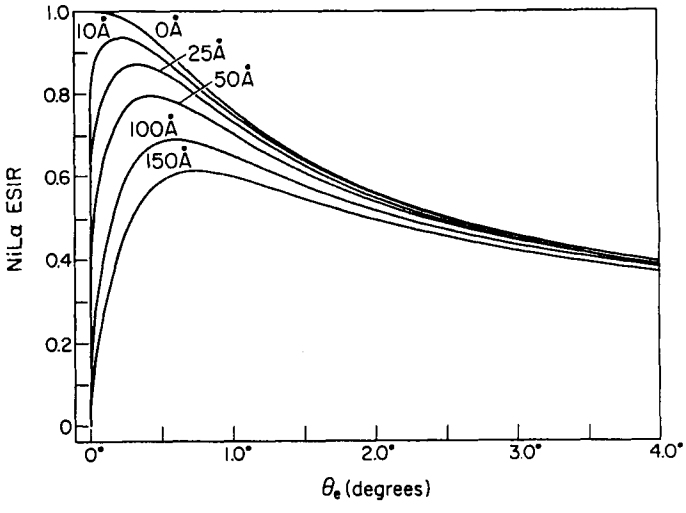

FIGURE 7. The Ni Lα ESIR is plotted as a function of exit angle for hydrocarbon contamination thicknesses ranging from 0 to 150 Å.

mental fluorescence production equation [Equation 1]), do not cancel for this intensity ratio. With these considerations in mind, one can derive an ISIR expression of the following form:

$$\frac{I_A}{I_B} = (A_t)(E_r)\left(\frac{\alpha_B}{\alpha_A}\right)\left[\frac{(1 - \exp(-\alpha\rho' t)_A)}{(1 - \exp(-\alpha\rho t)_B)}\right] \qquad (10)$$

where A_t is the appropriate attenuation factor for the A-B thin film system given by the Fi,j and Fe,j terms in Equation 8 and Er is the experimental ratio which corrects for different fundamental terms mentioned previously and is given by

$$E_r = \frac{[I_{A,\infty}(\Theta_e)][\alpha_A(\Theta_e)]}{[I_{B,\infty}(\Theta_e)][\alpha_B(\Theta_e)]}$$

The ISIR for a sample consisting of a variable Ni thickness over 150 Å of Fe is plotted in Figure 8. One can see the ISIR changes more dramatically than the ESIR at low angles since the Ni intensity increases and the Fe intensity decreases. Furthermore, one can more clearly differentiate between two different Ni thicknesses in the ISIR case. One can see how the ISIR changes as the Ni film is kept constant at 150 Å while the Fe thickness is varied. This is illustrated in Figure 9 and the same arguments for the variable Ni thickness case also hold true for this case.

While the ISIR partially compensates for contamination, the correction is not complete. If the absolute contamination thickness is tc, the ISIR between two layers A and B will be modified by a factor Ac which is

$$A_c = \exp[-(d\mu_{i,c}\csc\theta_i + d\mu_{e,c}\csc\theta_e)\rho_c t_c] \qquad (11)$$

where dμi,c and dμe,c are (μia,c-μib,c) and (μea,c-μeb,c),

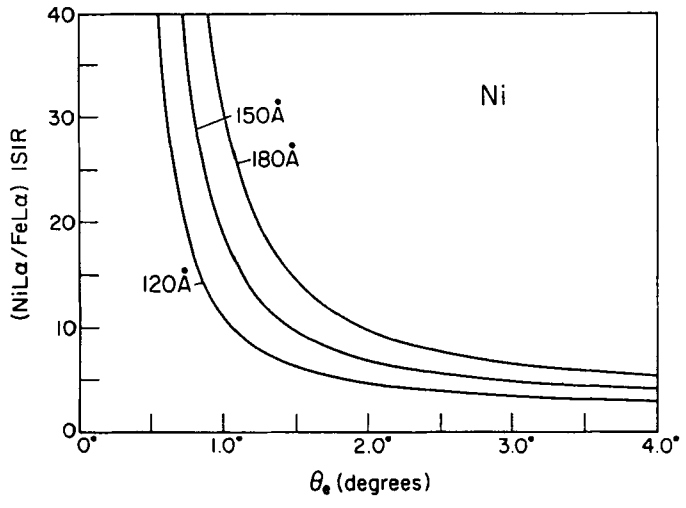

FIGURE 8. The Ni/Fe Lα internal standard intensity ratio (ISIR) is plotted as a function of exit angle for a Ni/Fe thin film where the Ni thickness is varied and the Fe thickness is held constant at 150 Å.

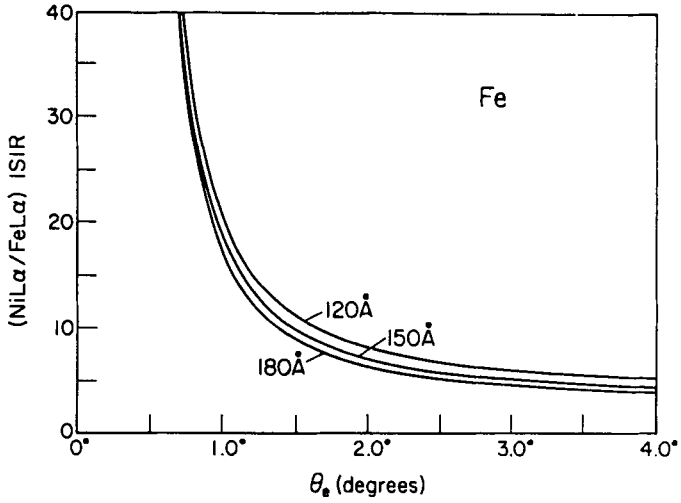

FIGURE 9. The Ni/Fe Lα ISIR is plotted as a function of exit angle for a Ni/Fe thin film where the Fe thickness is varied and the Ni overlayer thickness is held constant at 150 Å.

respectively. Furthermore, if the radiation is monochromatic, dμi,c = 0. The advantage in the ISIR method over the ESIR method, insofar as contamination is concerned, occurs in the grazing exit mode if (dμe,c)(tc) < (μe,c)dtc. The effect of contamination on the ISIR is illustrated in Figure 10 for a Ni/Fe 2 layer system (thickness for Ni and Fe is 150 Å each).

IV. INSTRUMENTAL ASPECTS

The ultrasoft X-ray fluorescence spectrometer used to demonstrate the grazing exit angle VAXFS technique has been described elsewhere.[11,25-27] A diagram of the instrument is shown in Figure 11. A Henke tube with an interchangeable anode is used as the excitation source. The Ni and Fe experimental

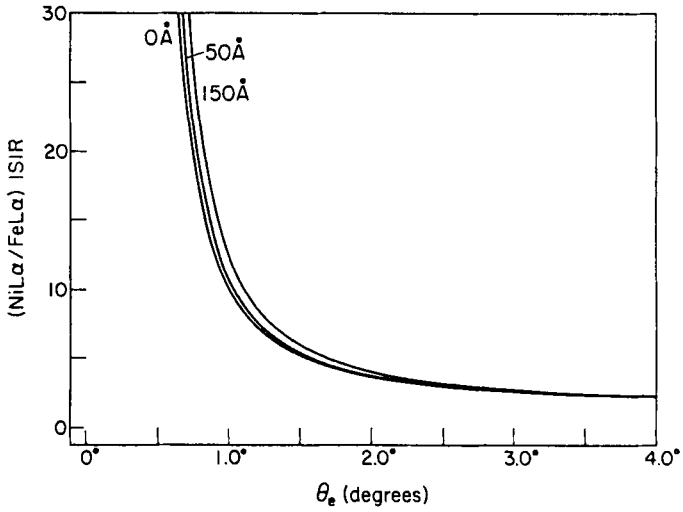

FIGURE 10. The Ni/Fe Lα ISIR is plotted for hydrocarbon contaminant thicknesses of 0, 50, and 150 Å.

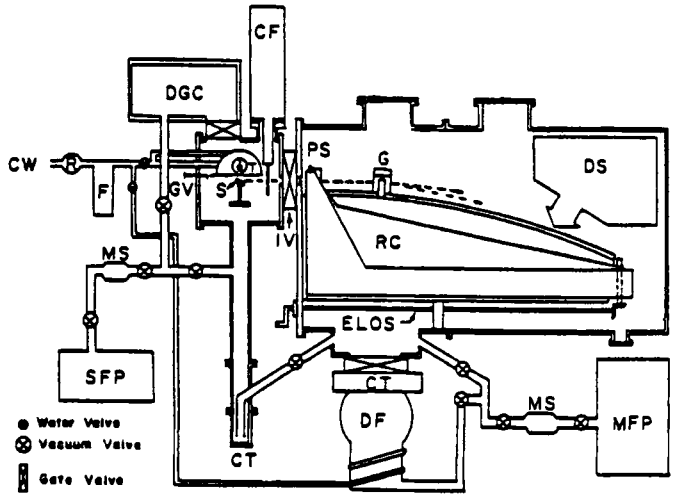

FIGURE 11. Mechanical block diagram of the 5-m grating X-ray spectrometer: RC-Rowland circle, G-grating, PS-primary slit, DS-detection system, IV-isolation valve between X-ray tube (T) and sample (S), CF-cold finger, DG-degassing sample chamber, ELOS-external line of sight, CW-cooling water, R-regulator, F-filter, MS-molecular sieve, CT-cold trap, SFP-sample chamber forepump, and MFP-main chamber forepump.

results presented here rely on the Cu anode with Cu Lα characteristic radiation exciting both Ni and Fe 2p electrons which give rise to Ni and Fe Lα radiation, respectively. The Cu L results rely on Al Kα excitation. A single channel thin window gas proportional counter was used in these measurements. The sample chamber operating pressure for this instrument is approximately 10^{-5} torr. The stability of the instrument was monitored by periodically monitoring the Lα intensity from a suitable standard (e.g., Ni, Fe, or Cu oxide) held in a two position sample holder.

The sample was manually rotated with mechanical backlash minimized by always rotating in the same direction and approximately 0.5° below the angle at which the measurement was taken. Furthermore, a lead weight was attached to the push-pull manipulator joined to the two position sample holder insuring reproducible exit angles within 0.25°. Each set of readings for the different samples was taken from the experimentally determined zero angle with a reproducibility of approximately 0.1°.

V. EXPERIMENTAL RESULTS AND DISCUSSION

A. Thin Film Elemental Analysis

1. Ni/Fe Thin Films

The Ni/Fe thin film variable exit angle work presented here is from well characterized samples provided by IBM. Details of this work are presented in Reference 28. The thin films examined are listed in Table 1. The motivation for this study is to evaluate the nondestructive VAXFS technique on a well-characterized thin film system that could not be addressed by a somewhat competitive nondestructive analytical technique-Rutherford backscattering (RBS). While X-ray fluorescence has been used to study thin films, the soft X-rays detected by this instrument made it feasible to study thin films of a much smaller thickness since the absorption coefficient is approximately 2 to 3 orders of magnitude greater for soft X-rays than for hard X-rays.[20]

Table 1

Study#	Sample#	Sample description (nominal thicknesses)
1	1	500 Å Ni/500 Å Fe/500 Å Ni/500 Å Fe/1 μ Au/300 Å Cr/Cu
	2	1000 Å Fe/1 μ Au/300 Å Cr/Cu
2	1	150 Å Ni/150 Å Fe/150 Å Ni/150 Å Fe/1 μ Au/300 Å Cr/Cu
		XPS Measurements
		XPS characterization
1	1	190 Å Contamination/470 Å Ni/600 Å Fe - rest of sample not analyzed.
1	2	150 Å Contamination/57% Fe and 43% Ni

In experiments 1 and 2, a polished Fe or Ni disc was used as the bulk reference for the thin films. A direct evaluation of the VAXFS technique could be made since some of the samples were subsequently analyzed by X-ray photoelectron spectroscopy (XPS) in a depth profiling mode.

The first sample in experiment 1 consisted of a four-layer Ni/Fe/Ni/Fe thin film system with Ni being the top layer and each layer nominally being 500 Å. The Ni Lα ESIR is plotted in Figure 12 with the points representing experimental data. The solid line is a theoretically calculated curve using Equation 10 based on each multilayer thin film thickness. The XPS determined layer thicknesses for a number of samples are also listed in Table 1 and were used for the theoretical calculations whenever available. The Ni Lα data was first taken at 30/30-μm slit widths; however, with the energy difference between Ni Lα and Fe Lα emission being rather large, much wider slit widths (with much greater intensity) could be tolerated. The Ni Lα ESIR for the sample at 100/100-μm slit widths is also plotted in Figure 12. The decrease in the Ni Lα ESIR at low exit angles is attributed to the 190 Å contaminant overlayer on the sample surface since the 100/100-μm Ni Lα ESIR was measured after the 30/30-μm Ni Lα ESIR work. The theoretical curve corresponding to the 30/30-μm measurement does not include a contaminant overlayer whereas the 100/100-μm measurement does include the 190 Å overlayer. The Fe Lα ESIR is plotted in Figure 13 for both the experimental data and the theoretically calculated curve. The photoemission spectrum for this sample with no sputtering in the contaminated region is given in Figure 14. The large inelastic tail at low electron kinetic energy as well as the sub-

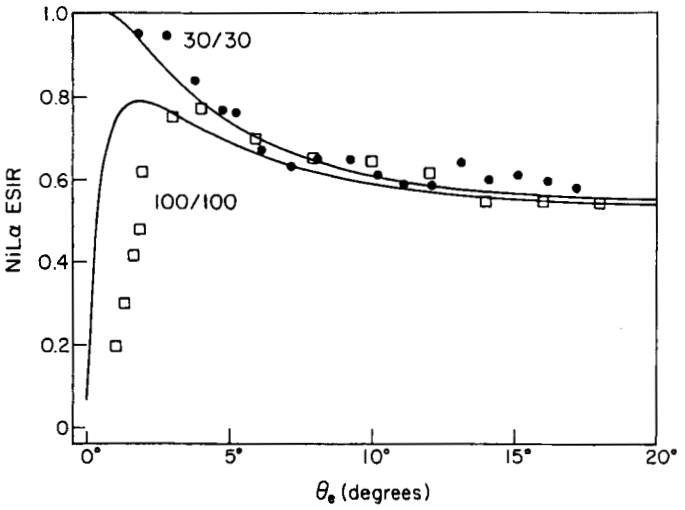

FIGURE 12. The Ni Lα ESIR is plotted as a function of exit angle for sample 1 in study 2. The theoretical curve (100/100 μm) assumes a contaminant overlayer thickness of 190 Å. The second curve (30/30) is calculated without any overlaying contaminant layer. The experimental data points for the 100/100-μm and 30/30-μm measurements are represented by □ and •, respectively.

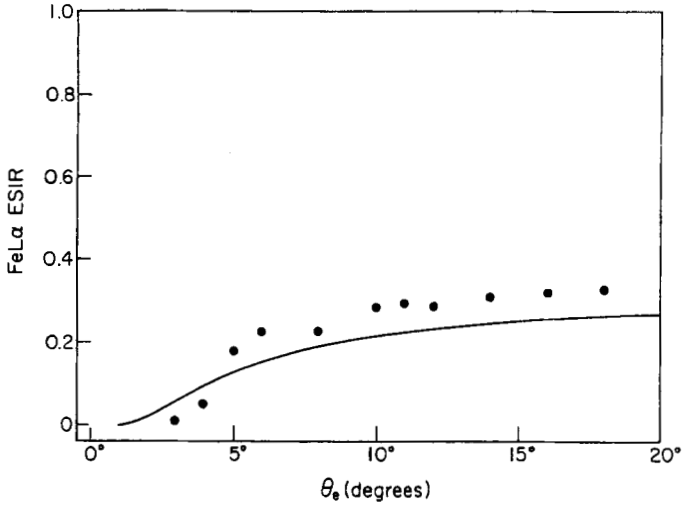

FIGURE 13. The Fe Lα ESIR is plotted as a function of exit angle for sample 1 in study 1 for a contaminant layer thickness of 190 Å.

stantial C 1s and O 1s signals indicates a large contaminant overlayer. The thickness of this overlayer, as well as the top Ni and Fe thin film layers was determined by an XPS depth profile. The depth profile of this sample at a spot where the X-rays irradiated the sample to a greater extent is given in Figure 15. One way of partially circumventing the problem of hydrocarbon contamination is to use Fe as an internal standard to correct for this preferential contamination. In this case, the Ni/Fe Lα ISIR ratio is plotted in Figure 16 with the solid line being the calculated curve (Equation 10).

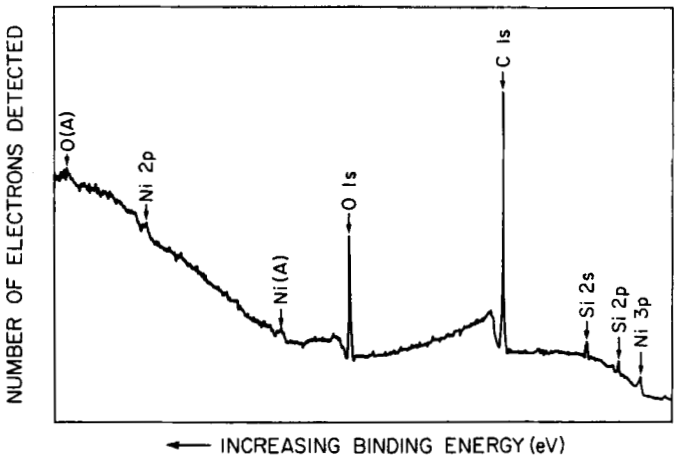

FIGURE 14. An XPS energy scan of sample 1 in study 1 in the contaminated region of the sample.

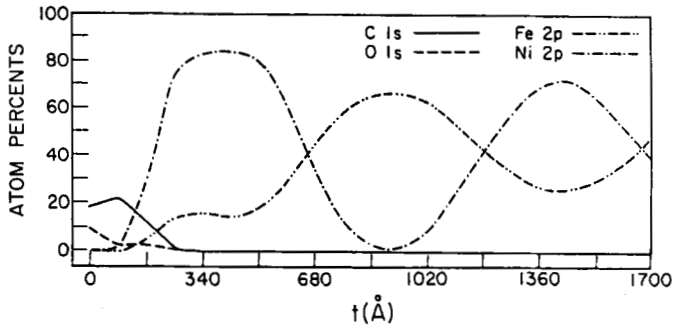

FIGURE 15. An XPS depth profile for sample 1 in study 1 in the contaminated region of the sample.

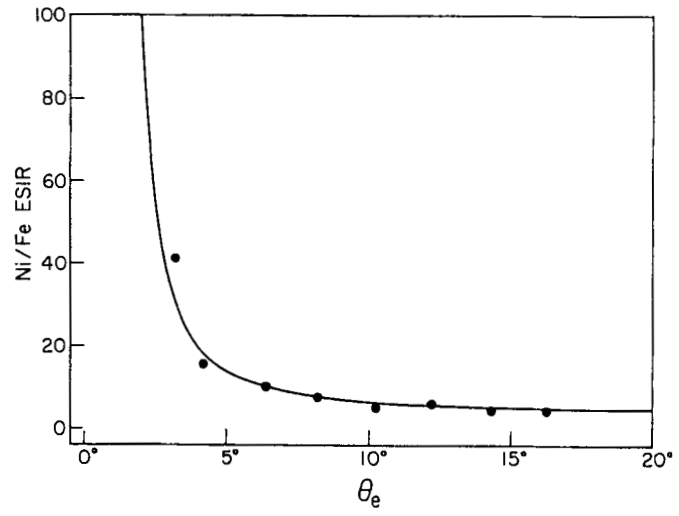

FIGURE 16. The Ni/Fe Lα ISIR is plotted as a function of exit angle for sample 1 in study 1 for a contaminant layer thickness of 190 Å.

While the contamination was an inconvenience in that different methods were devised to circumvent this problem, the previous result shows the ability of XFS to work nondestructively in a contaminated environment where other surface techniques appear hopeless. It should be mentioned that the contamination arose from the sample chamber and that the degree to which the samples in this experimental run were exposed to X-rays was roughly correlated to the hydrocarbon thickness overlayer. Finally, since a focused X-ray source was used in the photoemission work, one could scan over areas of the sample. By doing so, one could observe greater contamination in areas that had been exposed to the X-ray source used in the VEAXFS work. This is discussed in greater detail elsewhere.[28]

The next sample in experiment 1 was purportedly a 1000 Å Fe thin film. However, the disparity between the expected and obtained Fe Lα ESIR for this sample was so great that contamination within the Fe thin film layer was suspected. It was found that this sample was contaminated with Ni. The Ni Lα ESIR for a 1000 Å homogeneous thin film composed of 43% Ni and 57% Fe (compositions of Ni and Fe were subsequently determined by XPS) is plotted in Figure 17, while the Fe Lα ESIR for the same thin film is plotted in Figure 18. The Ni/Fe Lα ISIR for this sample is plotted in Figure 19 and the XPS depth profile is shown in Figure 20. The results on this sample demonstrate that the VAXFS technique is a sufficiently sensitive tool for monitoring the quality control of thin films.

The second experimental run corrected for some of the problems encountered in experiment 1. Special precautions were taken to reduce the amount of surface sample contamination. The slit widths used in this experiment were 60/60 μm as this was seen as a compromise since the Ni Lα Fe Lα interference was not too great and any correction to it could

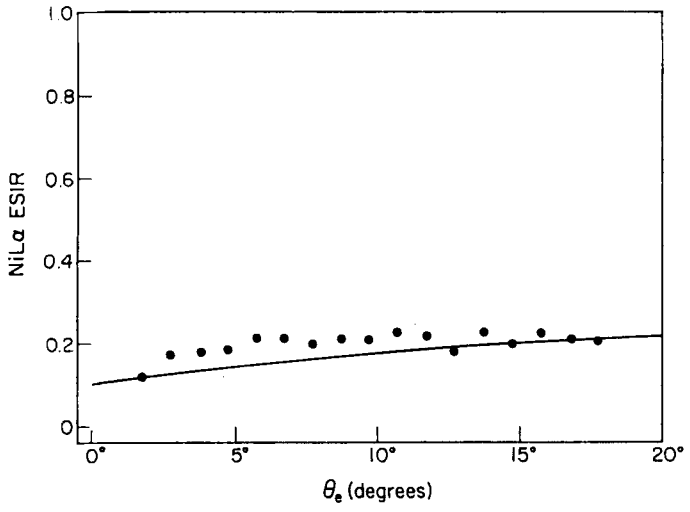

FIGURE 17. The Ni Lα ESIR is plotted as a function of exit angle for sample 2 in study 1 for no contaminant overlayer.

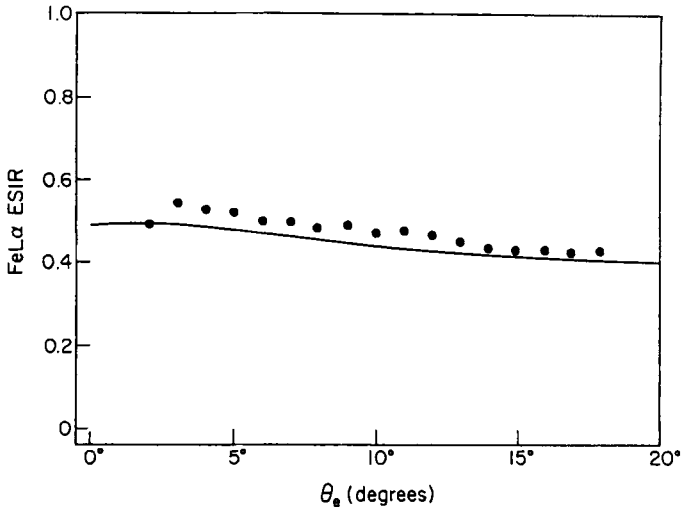

FIGURE 18. The Fe Lα ESIR is plotted as a function of exit angle for sample 2 in study 1 for no contaminant overlayer.

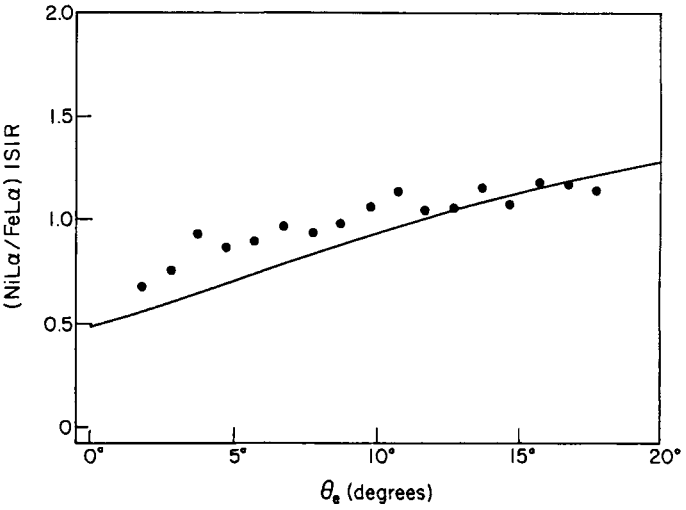

FIGURE 19. The Ni/Fe Lα ISIR is plotted as a function of exit angle for sample 2 in study 1 for no contaminant overlayer.

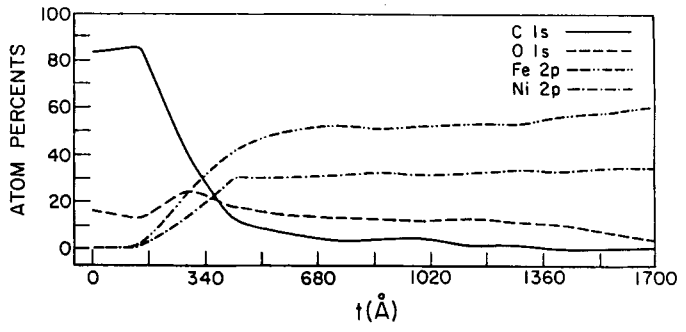

FIGURE 20. An XPS depth profile for sample 2 in study 1 in the contaminated region of the sample is shown.

be made with a fair degree of confidence. The results were also repeated at wider slit widths, and the agreement between the 60/60-μm and 100/100-μm slit widths was quite good, provided the Ni Lα optical background was corrected. The motivation for going to as high a slit width as possible comes about because the intensity gain on the instrument used in this experiment goes roughly at the square of the slit width. Therefore, the intensity at 60/60-μm slit widths is approximately four times greater than the intensity at 30/30-μm slit widths. This is especially important at low exit angles where sample self absorption diminishes the intensity to a large extent. The primary motivation for this experiment was to determine the potential for studying very thin films on the order of 100 Å.

The first sample consisted of a four-layer Ni/Fe thin film system with each thin films nominal thickness being 150 Å. The Ni Lα ESIR is plotted in Figure 21 with the plateau at low exit angles being attributed to preferential contamination. The Fe Lα ESIR for this sample is plotted in Figure 22 while the Ni/Fe Lα ISIR is plotted in Figure 23. These results demonstrate the success of the VEAXFS technique in analyzing thin films whose thickness is on the order of 100 Å. Furthermore, the good agreement between the theoretical curve and the experimental data demonstrates how well the experimental data can be predicted theoretically. The experimental work has thus far concentrated on elemental analysis. The discussion now turns to the analytical capability of analyzing chemically modified thin films by the VEAXFS technique.

B. Thin Film Chemical Analysis Work

1. The Lβ/Lα Technique

X-ray fluorescence and X-ray emission has been used as a chemical bonding and chemical speciation tool for quite some time. The Lβ/Lα technique is one such technique which can be used to monitor the chemical bonding changes in certain

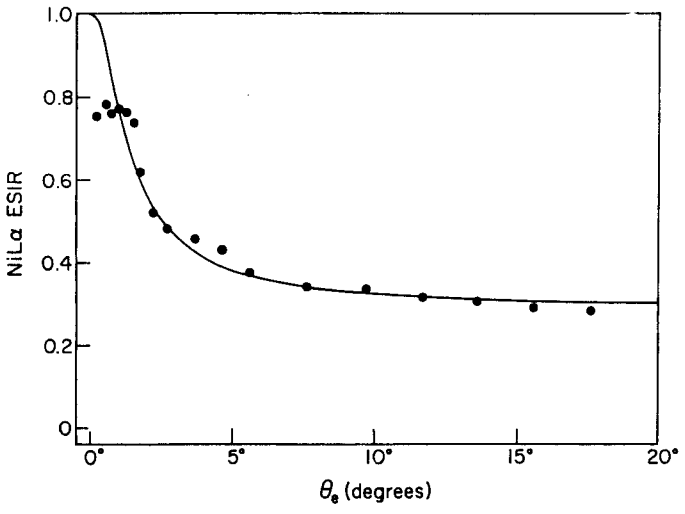

FIGURE 21. The Ni Lα ESIR is plotted as a function of exit angle for sample 1 in study 2 with no contaminant overlayer.

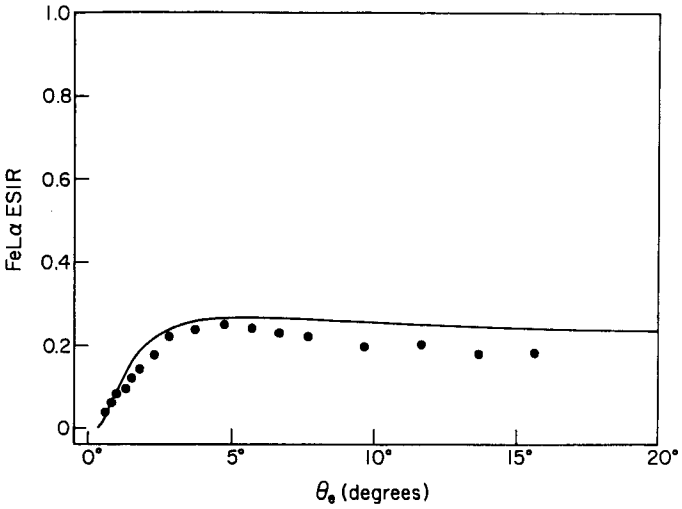

FIGURE 22. The Fe Lα ESIR is plotted as a function of exit angle for sample 1 in study 2 with no contaminant overlayer.

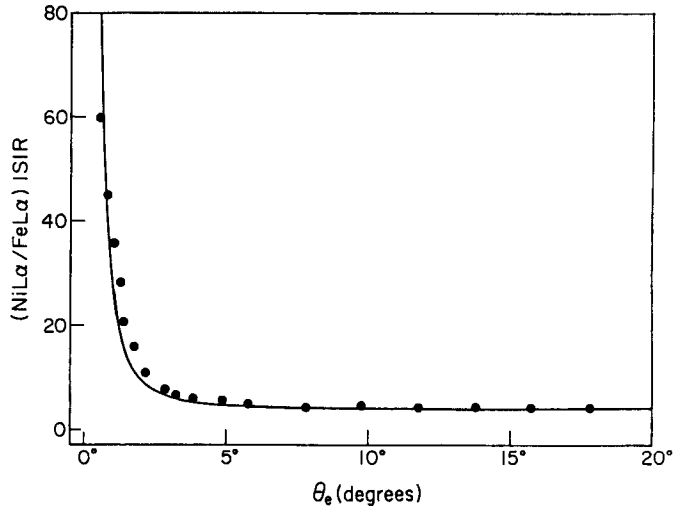

FIGURE 23. The Ni/Fe Lα ISIR is plotted as a function of exit angle for sample 1 in study 2 with no contaminant overlayer.

materials.[13,29] Since these X-rays are close in energy and are usually far from a contaminant absorption edge, they act as an internal standard correcting for surface contamination, roughness, etc. This technique also ignores the relative binding energy shifts that may be associated with the X-ray transitions of the different chemical states for a particular emitting atom. There are two reasons for neglecting these energy shifts. The first is that the chemically induced shifts are usually quite small and the second is that the instrumental resolution for this type of study is generally quite modest so that the peak spectrum is rather broad (but good enough to discern any chemical state changes). In the studies discussed next, a slit width of 30/30 μm was used, which for Fe Lα radiation translates to an instrumental resolution of approximately 4 eV.

The Lβ/Lα intensity ratio is a rather convenient ratio for characterizing the chemical state of 3d transition metals since this ratio is a function of the chemical state of the 3d transition metal. Fischer has found that by using electron excitation, the 3d transition metals Lβ/Lα intensity ratio changes as it is chemically modified.[29] The fundamental reasons for these spectral changes are discussed in Reference 30. Nevertheless, the emphasis here is on exploiting this spectral change to analyze a transition metal which has been chemically modified, as demonstrated by Holliday.[13]

2. Quantitative Treatment for Determining an Oxide Thickness as Applied to the Oxidation of Cu

The quantitative treatment for determining oxide thicknesses is rather straightforward, but is discussed in greater detail in Reference 30. For example, consider a sample consisting of three discrete layers with the top two layers being chemical modifications of the third layer (the substrate). The oxidation of Cu would be a realistic model for such a system in that the first, second, and third layers are CuO, Cu_2O, and Cu, respectively. In such a system where the Lβ/Lα intensity ratio is different for each Cu layer, the composite Lβ/Lα intensity ratio is simply:

$$\frac{L\beta}{L\alpha} = \sum_{i=1}^{3} \left(\frac{L\beta}{L\alpha}\right)_i I_f \qquad (12)$$

where I_f is the intensity fraction for the ith layer and is determined through the ordinary fluorescence equations (Equation 8) using available Lα absorption coefficients values.[20] The empirical Lβ/Lα intensity ratio for each ith material (layer) is also evaluated at the appropriate incident and exit angle.

The calculated Lβ/Lα ratio for various CuO and Cu_2O thicknesses is plotted in Figure 24. The decrease in the Lβ/Lα intensity ratio is attributed to sample self absorption. From such a plot, the degree to which the oxide thickness can be ascertained is quite good. For example, with a Cu_2O thickness of 50 Å one can experimentally discern 10 Å increments.

The agreement between the theoretical calculations (Equation 12) and the experimental results for Cu is quite good. For example, the ambient oxidation of Cu can be characterized by the VEAXFS technique employing the Lβ/Lα technique. The results of Cu substrate oxidized in atmosphere are shown in Figure 25, with the best fit between the calculated curve and experimental results corresponding to 0 Å of CuO and 70 Å of Cu_2O. The oxidation of Cu is discussed in greater detail in References 30 and 31.

The VEAXFS technique has also been used to study the oxidation of Fe[32] and Ni[11] as well, providing information on the extent to which these two transition metals form discrete oxide layers. This is discussed in further detail elsewhere.[11,32]

VI. FUTURE PROSPECTS

While XFS has become the method of choice as an elemental analysis tool, its use as a practical chemical bonding tool and as a nondestructive depth profiling probe has been mostly overlooked. The future prospects of this technique appear bright, especially in the soft ($\lambda > 10$ Å) X-ray region, and as detectors[33] and X-ray instrumentation in general (e.g., gratings, etc.) become more advanced.

VII. CONCLUSIONS

These variable angle experiments done in both elemental and chemical bonding modes demonstrate the utility of the VEAXFS technique. The chemical bonding and chemical speciation capability of X-ray emission (fluorescence) is partic-

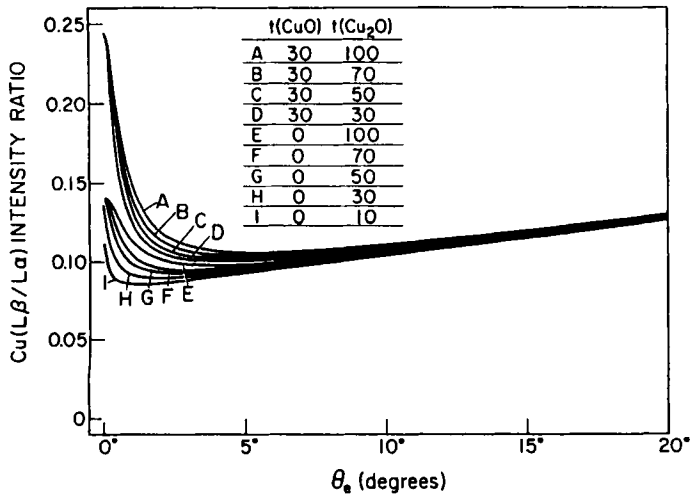

FIGURE 24. The Cu Lβ/Lα intensity ratio is plotted as a function of CuO and Cu_2O thicknesses, illustrating the resolution attainable by this method.

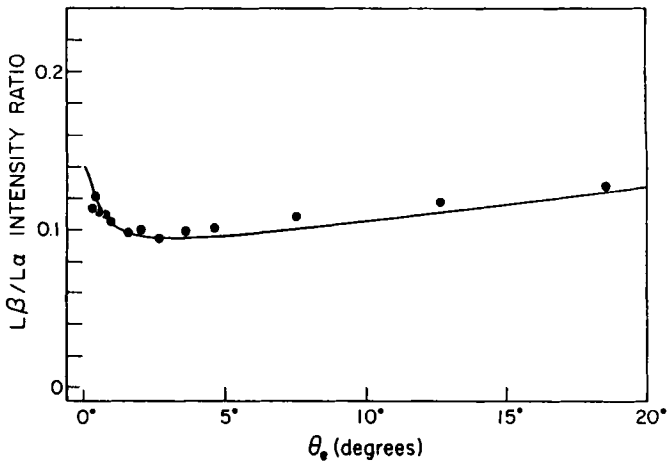

FIGURE 25. The Cu Lβ/Lα intensity ratio is plotted as a function of exit angle for an oxidized Cu substrate of 0 Å of CuO and 70 Å of Cu_2O.

ularly attractive since many of the thin film and surface probes available today are not able to provide such a capability. These studies also show that X-ray intensity distributions, intensity ratios, etc., can be rather easily calculated and can be compared to experimental results. Finally, this technique has a number of other advantages since it is a photon in-photon out experimental tool which is capable of directly probing the localized electron structure of a given material over a range of depths and in a variety of environments.

VIII. ACKNOWLEDGMENTS

I would like to thank C. R. Brundle for his help in the photoemission work discussed in this article. I would also like to acknowledge George Andermann for introducing me to this field, and collaboration with W. K. Kuhn on the Cu oxidation work is also acknowledged.

REFERENCES

1. **Morgan, A. E. and Werner, H. W.,** *Phys. Scripta,* 18, 451, 1978.
2. **Brundle, C. R.,** *J. Vac. Sci. Technol.,* 11, 212, 1974.
3. **Science Updata-Analytical Chemistry, C. & E. N.,** Nov. 29, 22, 1982.
4. **Marra, W. C., Eisenberger, P., and Cho, A. Y.,** *J. Appl. Phys.,* 50, 6927, 1979.
5. **Heald, S. M., et al.,** *Phys. Lett. A,* 103A(3), 155, 1984.
6. **Andre, J. M., Maquet, A., and Barchewitz, R.,** *Phys. Rev. B,* 25(9), 5671, 1982.
7. **Iida, A., Sakurai, K., Yoshinaga, A., and Gohshi, Y.,** *Nucl. Instr. Methods,* A246, 736, 1986.
8. **Manne, R.,** *J. Chem. Phys.,* 52(11), 5733, 1970.
9. **Nefedov, V. I.,** *J. Struct. Chem.,* 12(2), 276, 1971.
10. **Andermann, G. and Fujiwara, F.,** *Anal. Chem.,* 52, 1711, 1984.
11. **Andermann, G.,** *Appl. Surf. Sci.,* 31, 1, 1988.
12. **Sakurai, K., Iida, A., and Gohshi, Y.,** *Jpn. J. Appl. Phys.,* 26(11), 1937, 1987.
13. **Holliday, J. E.,** *Adv. X-ray Anal.,* 16, 53, 1966.
14. **Szasz, A. and Kohnok, J.,** *Appl. Surf. Sci.,* 24, 34, 1985.
15. **Johansson, S. V. and Johansson, T. B.,** *Nucl. Instr. Methods,* 137, 473, 1976.
16. **Willis, J. E.,** *Adv. X-ray Anal.,* 31, 175, 1988.
17. **Huang, T. C. and Parrish, W.,** *Adv. X-ray Anal.,* 29, 395, 1986.
18. **Mantler, M.,** *Anal. Chim. Acta,* 188, 25, 1986.
19. **Bertin, E. P.,** *Principles of X-Ray Spectrometric Analysis,* 2nd ed., Plenum Press, 1975.
20. **Henke, B. L., Lee, P., Tanaka, T. J., Shimabukuro, R. L., and Fujikawa, B. K.,** *Atomic Data Nucl. Data Tables,* 27, 1-44, 1982.
21. **Scimeca, T. and Andermann, G.,** General theoretical treatment of the angular dependence of critical depths in X-ray fluorescence spectroscopic studies of surfaces, thin films and multilayers, accepted for publication in *Surf. Interfac. Anal.*
22. **Bambynek, W., et al.,** *Rev. Modern Phys.,* 44(4), 716, 1972.
23. **Kuhn, K. and Andermann, G.,** Effects of surface roughness on surface analysis via soft and ultrasoft X-ray fluorescence spectroscopy, in preparation.
24. **Scimeca, T. and Andermann, G.,** *Surf. Interfac. Anal.,* 10, 321, 1987.
25. **Andermann, G., Bergknut, L., Karras, M., and Grieshaber, G.,** *Rev. Sci. Instr.,* 51, 814, 1980.
26. **Andermann, G., Bergknut, L., Karras, M., and Grieshaber, G.,** *Spec. Lett.,* 11, 571, 1978.
27. **Andermann, G., Burkard, F., Kim, R., Fujiwara, F., and Karras, M.,** *Spec. Lett.,* 16, 891, 1983.
28. **Scimeca, T., Andermann, G., and Brundle, C. R.,** in preparation.
29. **Fischer, D. W.,** *J. Appl. Phys.* 36(6), 2048, 1964.
30. **Scimeca, T., Andermann, G., and Kuhn, W. K.,** The quantitative characterization of the oxidation of Cu by variable exit angle ultrasoft X-ray fluorescence spectroscopy, accepted for publication in *Appl. Surf. Sci.*
31. **Kuhn, K. and Andermann, G.,** The use of ultrasoft X-ray fluorescence as a tool to characterize the oxidation of Cu, in preparation for submission to *Surf. Interfac. Anal.*
32. **Scimeca, T. and Andermann, G.,** The oxidation of Fe as characterized by variable exit angle X-ray fluorescence, in preparation.
33. **Callcott, T. A., Tsang, K. L., Zhang, C. H., Ederer, D. L., and Arakawa, E. T.,** *Rev. Sci. Instrum.,* 57, 2680, 1986.